Robust fault-tolerant control for switched systems based on interval observer fault diagnosis and interval dynamic event-triggered mechanism

Xingjian Fu, Xiaohan Wang

School of Automation, Beijing Information Science and Technology University, 100192, Beijing, China
(e-mail: fxj@bistu.edu.cn, wwxxhh981118@163.com)

Abstract: In this paper, an interval observer-based fault diagnosis mechanism and an interval dynamic event-triggered robust fault-tolerant control strategy are proposed for uncertain nonlinear switched systems. Firstly, the interval observer design problem is transformed into a Sylvester equation solution problem by introducing the coordinate transformation method in the absence of actuator faults, and the corresponding interval observer design method is given. Secondly, based on the interval observer output, upper and lower bound estimates of the system outputs are constructed, and fault diagnosis is realized by monitoring whether the system output exceeds the preset bounds. In addition, an improved interval dynamic event triggered mechanism is proposed to optimize the utilization of communication and computational resources and reduce redundant information transmission. The mechanism incorporates interval estimation information and real-time residuals, which can effectively extend the triggering time interval while improving the fault detection performance. Based on the interval fault diagnosis results, a fault-tolerant control strategy based on the interval dynamic event triggered mechanism is proposed, and the conditions for asymptotic stabilization of the closed-loop system are given. Finally, a nonlinear model of a morphing aircraft system with variable wing curvature is used to verify the validity of the designed scheme.

Keywords: interval observer; fault detection; Interval dynamic event triggered mechanism; robust fault-tolerant control; switched system

1. INTRODUCTION

With the increasing complexity of industrial systems, safety and reliability have become one of the core elements in control system design. Therefore, for the safety and high reliability of the system to be ensured, various types of potential faults must be comprehensively considered, and advanced technical means along with complex control strategies are required to be utilized for their effective handling. The importance of Fault Detection (FD) and Fault Tolerant Control (FTC) techniques has been demonstrated in the improvement of control system performance and stability, particularly when various types of faults are encountered by the system. It is noteworthy that among the more popular fault detection methods include: filter-based fault detection techniques (Zheng et al., 2004; Szaszi et al., 2002), observer-based fault detection techniques (Li et al., 2019; Commault et al., 2002; Zhu et al., 2020a) and parity space fault detection techniques (Shuai et al., 2020; Wang et al., 2017). Among them, observer-based fault detection techniques have become one of the most important fault detection methods at present. In this method, the observer is usually designed as a fault detector, which is robust to system disturbances and at the same time exhibits high sensitivity to faults. A residual signal is generated from the output of the observer to achieve effective detection of faults. By comparing the residuals to a fixed or adaptive threshold, it is possible to determine whether the system is failing in some way. The problem of fault detection and estimation in DC-DC converter based switched systems was studied in (Li et al., 2019). A sliding mode observer (SMO) is designed to generate residual signals to be compared with a set threshold value for the fault detection purpose. Meanwhile, the fault estimation is realized by the fault reconstruction method. The problem of fault detection and isolation (FDI) for linear systems with faults and disturbances was considered in (Commault et al., 2002). A set of observer-based residuals is designed such that the transfer from disturbances to residuals is zero and the transfer from faults to residuals permits fault isolation. The problem of simultaneous estimation of state, actuator and sensor faults for a class of uncertain switched systems and the design of observer-based fault-tolerant control was studied in (Zhu et al., 2020a). By designing a dimensionality-reducing observer, simultaneous estimation of the state, actuator faults and sensor faults of the original system can be realized without being affected by disturbances. And based on the state estimation obtained from the reduced dimensional observer, a state-fault feedback fault-tolerant controller based on optimized $H_{\infty/-}$ performance metrics is designed.

Switched systems, as a very important special type of hybrid system, can be described as consisting of a finite number of continuous (or discrete) time subsystems and a switched strategy that determines the dynamic behavior of the system. In practical engineering, switched systems have been widely used in many fields, such as: robotic power systems, wind power generation systems, variant aircraft control systems (Liu et al., 2019; Zhu et al., 2020; Han et al., 2015; Chen and Francis, 2012), etc., which has prompted the study of nonlinear switched systems to become an increasingly important topic in control theory. In a switched system, the system state may be switched between different modes, resulting in an increase in the complexity of fault detection. Conventional fault detection methods face many challenges, especially in environments with large dynamic changes and uncertainties. Therefore, the development of a technology capable of accurately and real-timely monitoring the system status and timely recognizing faults is considered particularly important.

With the development of interval observer theory, an ideal solution has been provided by this tool for state estimation and fault detection (Zhang and Yang, 2018; Guo and Zhu, 2016; Pourasghar et al., 2016; Meseguer et al., 2010). Constraints on the dynamics are provided by the interval observer through the construction of upper and lower bounds on the state estimation, which are enabled to generate residual signals and provide implicit thresholds for fault diagnosis. In this approach, the complex steps of residual evaluator and threshold selector in the traditional observer design are omitted, resulting in a more concise and intuitive overall process. In (Zhang and Yang, 2018), a set of FDI interval observers is constructed by considering both local outputs and outputs received from neighboring multi-agents. The observer gains are determined through simultaneous solutions of disturbance attenuation, fault sensitivity, and non-negative conditions. In (Guo and Zhu, 2016), a fault detection method is developed for nonlinear systems containing actuator faults with simultaneous uncertainties and external disturbances, where an interval observer is utilized for the construction of corresponding residuals. In (Pourasghar et al., 2016), a fault diagnosis isolation (FDI) strategy has been developed for fuzzy interconnected systems with unknown interconnections through the utilization of interval observers. Furthermore, the accuracy of fault detection is significantly influenced by modeling uncertainty. When an interval observer is used, the minimum detectable fault is highly dependent on the observer gain, as described in (Meseguer et al., 2010).

Currently, the research on nonlinear systems is gradually focusing on practical application scenarios, and event-triggered control (ETC) is an important direction. ETC has received much attention due to its ability to effectively reduce computation and communication costs while maintaining good performance (Wu et al., 2021; Ma et al., 2020a; Ding et al., 2019). Switched systems are widely used in network-dependent information transfer, facing bandwidth constraints and additional resource utilization. Therefore, it is especially important to introduce event triggering mechanism in the switched system (Xiao et al., 2018; Qi et al., 2021). A mode-dependent event-triggered transmission scheme based on pattern correlation was proposed in (Xiao et al., 2018), modeling the closed-loop system as a switched system with delayed states and enhanced switched signals. Then, exponential stabilization conditions characterized by the residence time and average residence time of the switched signals are obtained for sampling data control of the non-switched system. In (Qi et al., 2021), an adaptive event-triggered scheme with a switched structure is used to achieve better adjustment of the triggering frequency. A systematic framework for analyzing the stability of multi-asynchronous switched and solving the controller gain is also established.

For the further reduction of communication resource consumption, the dynamic event-triggered mechanism has been developed. In comparison with the static event- triggered mechanism, internal dynamic variables have been introduced into the static triggering conditions in (Girard, 2014; Ge and Han, 2017). A larger trigger interval and a reduced number of triggers are able to be realized by this method while system performance is maintained. At present, many researchers have conducted in-depth studies on the application of event-triggered mechanisms, which have achieved fruitful results and are widely used in the solution of various problems (Ma et al., 2020b; Long and Wang, 2021; Long et al., 2022). In (Ma et al., 2020b), a dynamic event triggered strategy and quantization control are used to adjust the signal transmission to reduce the transmission load. Unlike the existing dynamic event triggered strategies, the triggering conditions only need to be monitored at discrete times. In addition, a state-dependent switched law is designed using only discrete state information. The sufficient conditions are given to guarantee the H_∞ performance under event-triggered sampling, quantization control and state-dependent switched conditions. In (Long and Wang, 2021), the dynamic event-triggered adaptive neural network control problem for a class of switching strict feedback uncertainty nonlinear systems is investigated. A novel dynamic event-triggered adaptive neural network control strategy based on the switching command filter is established by utilizing the backstepping method and command filter, and the difficulty of the error discontinuity in the switching measurement is overcome by introducing the segmentation constant variable. Robust adaptive event-triggered control for nonlinear switched systems is explored in (Long et al., 2022). In the study, a robust adaptive controller under dwell time switched is designed using the backstepping method, and the event triggering mechanism is integrated into the switched controller. Through this approach, the Zeno behavior is effectively avoided, and the global asymptotic stability of the system is ensured.

However, the existing dynamic conditions are often dependent on fixed parameters or simple state variables, and the state information of the system is not fully utilized. Therefore, in this paper, a novel interval dynamic event triggered strategy is proposed, based on the original triggering conditions, a new triggering condition is designed by interval estimation information and real-time residuals. The number of triggers can be further reduced while system performance is maintained, and Zeno behavior will not occur. The main contributions of this paper can be summarized as follows. (1) Fault detection for nonlinear switched systems with external perturbations, actuator faults, and uncertainties is achieved by designing interval observers. (2) The interval dynamic event triggering mechanism is designed based on the interval estimation information as well as the real-time residuals, which greatly reduces the number of communications and excludes the Zeno behavior. (3) The robust fault-tolerant controller is designed based on the fault diagnosis results, and the conditions for asymptotic stabilization of the closed-loop system are given. At last, the validity of the scheme is verified by nonlinear simulation for the morphing aircraft system with variable wing curvature used in (Zhu and Yu, 2022).

The paper is organized as follows. The problem description is provided in Section II. The design of interval observer and fault diagnosis is given in Section III. The interval dynamic event triggering mechanism and robust fault-tolerant controller are designed in Section IV. Simulation results are given in Section V to illustrate the effectiveness of the design. Finally, conclusions are presented in Section VI.

2. DESCRIPTION OF PROBLEM

Consider the following nonlinear switched system:

$$\begin{cases} \dot{x}(t) = (A_\sigma + \Delta A_\sigma)x(t) + B_\sigma u(t) + E_\sigma S_a(t) \\ + f_\sigma(x,t) + D_\sigma \omega(t) \\ y(t) = C_\sigma x(t) \end{cases} \tag{1}$$

where $\sigma : R^+ \to N\{1,2,\cdots,n\}$ is the switched law, which is a piecewise constant function that depends on the state or time. $\Delta A_\sigma, y(t), u(t), x(t), S(t), \omega(t)$ represent unknown but bounded system uncertainties, output variables, input variables, state variables, actuator failures, and unknown external disturbances, respectively. There exists a known boundary for the system uncertainty parameter ΔA_σ satisfying $\Delta \underline{A}_\sigma \le \Delta A_\sigma \le \Delta \overline{A}_\sigma$. $A_\sigma, B_\sigma, C_\sigma, D_\sigma, E_\sigma$ are matrices of the known real constants with appropriate dimension.

Assumption 1 (A_σ, B_σ) is controllable, (A_σ, C_σ) is observable.

Assumption 2 For the initial state of the system $x(0)$, there exist known vectors $\overline{x}(0), \underline{x}(0)$,satisfying $\underline{x}(0) \le x(0) \le \overline{x}(0)$. For the unknown external perturbation $\omega(t)$, there exist known upper and lower bounds $\overline{\omega}(t), \underline{\omega}(t)$, satisfying $\underline{\omega}(t) \le \omega(t) \le \overline{\omega}(t)$.

Assumption 3 For any $\sigma \in N$, f_σ is a known nonlinear function that is monotonically increasing with respect to x and satisfies the global Lipschitz condition, for all $t \ge 0$, there are

$$\| f_\sigma(x,t) \| \le \theta \| x_1 - x_2 \| \tag{2}$$

where θ is the known Lipschitz positive constant, $x_1 \in R^n$ and $x_2 \in R^n$ are any two variables.

Lemma 1(Efimov and Raïssi, 2016) For a vector $x(t) \in R^n$, there exist known vectors $\overline{x}(t), \underline{x}(t) \in R^n$, such that $\underline{x}(t) \le x(t) \le \overline{x}(t)$. if $A \in R^{m \times n}$ is a nonnegative matrix, and there exist $\overline{A}, \underline{A} \in R^{m \times n}$ satisfying $\underline{A} \le A \le \overline{A}$, then there are

$$\begin{aligned} &\underline{A}^+ \underline{x}^+ - \overline{A}^+ \underline{x}^- - \underline{A}^- \overline{x}^+ + \overline{A}^- \overline{x}^- \le Ax(t) \\ &\le \overline{A}^+ \overline{x}^+ - \underline{A}^+ \overline{x}^- - \overline{A}^- \underline{x}^+ + \underline{A}^- \underline{x}^- \end{aligned} \tag{3}$$

Lemma 2 (Guo et al., 2019) For a vector $x \in R^n$,there exist known vectors $\overline{x}(t), \underline{x}(t) \in R^n$, such that $\underline{x}(t) \le x(t) \le \overline{x}(t)$, if $A \in R^{m \times n}$ is a non-negative matrix, then the following inequality holds

$$A\underline{x}(t) - A\overline{x}(t) \le Ax(t) \le A\overline{x}(t) - A\underline{x}(t) \tag{4}$$

Lemma 3 (Cui and Xiang, 2022) For any matrices A and B with appropriate dimensions, the following inequality holds

$$A^T B + B^T A \le \gamma A^T A + \frac{1}{\gamma} B^T B \tag{5}$$

where γ is the known positive constant.

Lemma 4 (Ashraf et al., 2021) x and y are two variables. For a positive scalar μ and a symmetric positive definite matrix $G > 0$, the following inequality holds

$$2x^T y \le \frac{1}{\mu} x^T G x + \mu y^T G^{-1} y \quad x, y \in R \tag{6}$$

Lemma 5 (Guo and Zhu, 2016) For a continuous system $\dot{x}(t) = Ax(t) + w(t)$, $w(t)$ is unknown external disturbance, if $x(0) \ge 0$,then for $\forall t \ge 0$,there must be $x(t) \ge 0$,where $A \in R^{m \times n}$ is a non-negative matrix.

In **Lemma** 5, a square matrix A is said to be a Hurwitz matrix if all of its eigenvalues have negative real parts, and a Schur matrix if all of the eigenvalue norms of the square matrix A are less than one.

3. DESIGN OF INTERVAL OF OBSERVER

For the system (1) , the parameter uncertainty term is given by Lemma 1

$$\begin{aligned} &\Delta \underline{A}^+ \underline{x}^+ - \Delta \overline{A}^+ \underline{x}^- - \Delta \underline{A}^- \overline{x}^+ + \Delta \overline{A}^- \overline{x}^- \le \Delta A x(t) \\ &\le \Delta \overline{A}^+ \overline{x}^+ - \Delta \underline{A}^- \overline{x}^- - \Delta \overline{A}^- \underline{x}^+ + \Delta \underline{A}^- \underline{x}^- \end{aligned} \tag{7}$$

let

$$\begin{cases} \underline{\kappa}(\overline{x}, \underline{x}, \Delta \overline{A}, \Delta \underline{A}) = \Delta \underline{A}^+ \underline{x}^+ - \Delta \overline{A}^+ \underline{x}^- - \Delta \underline{A}^- \overline{x}^+ + \Delta \overline{A}^- \overline{x}^- \\ \overline{\kappa}(\overline{x}, \underline{x}, \Delta \overline{A}, \Delta \underline{A}) = \Delta \overline{A}^+ \overline{x}^+ - \Delta \underline{A}^- \overline{x}^- - \Delta \overline{A}^- \underline{x}^+ + \Delta \underline{A}^- \underline{x}^- \end{cases} \tag{8}$$

The above equation is organized to yield

$$\underline{\kappa}(\overline{x}, \underline{x}, \Delta \overline{A}, \Delta \underline{A}) \le \Delta A x(t) \le \overline{\kappa}(\overline{x}, \underline{x}, \Delta \overline{A}, \Delta \underline{A}) \tag{9}$$

The Luenberger-type interval observer for system (1) is designed as follows:

$$\begin{cases} \dot{\overline{x}}(t) = (A_\sigma - LC_\sigma)\overline{x}(t) + B_\sigma u(t) + Ly(t) + {D_\sigma}^+ \overline{\omega}(t) \\ -{D_\sigma}^- \underline{\omega}(t) + f(t, \Delta \overline{x}) + \overline{\kappa}(\overline{x}, \underline{x}, \Delta \overline{A}, \Delta \underline{A}) \\ \dot{\underline{x}}(t) = (A_\sigma - LC_\sigma)\underline{x}(t) + B_\sigma u(t) + Ly(t) + {D_\sigma}^+ \underline{\omega}(t) \\ -{D_\sigma}^- \overline{\omega}(t) + f(t, \Delta \underline{x}) + \underline{\kappa}(\overline{x}, \underline{x}, \Delta \overline{A}, \Delta \underline{A}) \end{cases} \tag{10}$$

where ${D_\sigma}^+ = \max\{0, D_\sigma\}, {D_\sigma}^- = {D_\sigma}^+ - D_\sigma$ $f(t, \Delta \overline{x}) = f(t, \overline{x})$ $- f(t, \underline{x}), f(t, \Delta \underline{x}) = f(t, \underline{x}) - f(t, \overline{x})$.

Take $\psi(t) = Tx(t)$, T is an invertible constant matrix. Let $S_a(t) = 0$, then system (1) can be rewritten as

$$\begin{cases} \dot{\psi}(t) = TA_\sigma T^{-1} \psi(t) + TB_\sigma u(t) + TD_\sigma \omega(t) \\ + Tf_\sigma(t,x) + T\kappa(T^{-1}\psi, \Delta A) \\ y(t) = CT^{-1}\psi(t) \end{cases} \tag{11}$$

If the inequality (7) is satisfied by the system (10), then a similar property is possessed by $T\lambda(T^{-1}\psi, \Delta A)$ for system (11). Under this condition, it follows from Lemma 2 that

$$\begin{aligned} &\underline{\eta} = T^+ \underline{\zeta}(\overline{x}, \underline{x}, \Delta \overline{A}, \Delta \underline{A}) - T^- \overline{\zeta}(\overline{x}, \underline{x}, \Delta \overline{A}, \Delta \underline{A}) \\ &\le T\kappa(T^{-1}\psi, \Delta A) \\ &\le T^+ \overline{\zeta}(\overline{x}, \underline{x}, \Delta \overline{A}, \Delta \underline{A}) - T^- \underline{\zeta}(\overline{x}, \underline{x}, \Delta \overline{A}, \Delta \underline{A}) = \overline{\eta} \end{aligned} \tag{12}$$

where

$$\begin{cases}\bar{\zeta}(\bar{x},\underline{x},\Delta\bar{A},\Delta\underline{A})=\bar{\lambda}((T^{-1})^{+}\bar{\psi}-\\(T^{-1})^{-}\underline{\psi},(T^{-1})^{-}\underline{\psi}-(T^{-1})^{+}\bar{\psi},\Delta\bar{A},\Delta\underline{A})\\=\Delta\bar{A}^{+}((T^{-1})^{+}\bar{\psi}-(T^{-1})^{-}\underline{\psi})^{+}-\Delta\underline{A}^{+}((T^{-1})^{+}\bar{\psi}-(T^{-1})^{-}\underline{\psi})^{-}\\-\Delta\bar{A}^{-}((T^{-1})^{+}\underline{\psi}-(T^{-1})^{-}\bar{\psi})^{+}+\Delta\underline{A}^{-}((T^{-1})^{+}\underline{\psi}-(T^{-1})^{-}\bar{\psi})^{-}\\\underline{\zeta}(\bar{x},\underline{x},\Delta\bar{A},\Delta\underline{A})=\underline{\lambda}((T^{-1})^{+}\bar{\psi}-\\(T^{-1})^{-}\underline{\psi},(T^{-1})^{-}\underline{\psi}-(T^{-1})^{+}\bar{\psi},\Delta\bar{A},\Delta\underline{A})\\=\Delta\underline{A}^{+}((T^{-1})^{+}\underline{\psi}-(T^{-1})^{-}\bar{\psi})^{+}-\Delta\bar{A}^{+}((T^{-1})^{+}\underline{\psi}-(T^{-1})^{-}\bar{\psi})^{-}\\-\Delta\underline{A}^{-}((T^{-1})^{+}\bar{\psi}-(T^{-1})^{-}\underline{\psi})^{+}+\Delta\bar{A}^{-}((T^{-1})^{+}\bar{\psi}-(T^{-1})^{-}\underline{\psi})^{-}\end{cases} \tag{13}$$

Therefore, without considering the effect of actuator failure, the interval observer can be designed as

$$\begin{cases}\dot{\bar{\psi}}(t)=TA_{\sigma}T^{-1}\bar{\psi}(t)+TB_{\sigma}u(t)+TL(y-CT^{-1}\bar{\psi}(t))+\\\qquad[(TD_{\sigma})^{+}\bar{\varpi}(t)-(TD_{\sigma})^{-}\underline{\varpi}(t)]+Tf_{\sigma}(t,\Delta\bar{x})+\bar{\eta}\\\dot{\underline{\psi}}(t)=TA_{\sigma}T^{-1}\underline{\psi}(t)+TB_{\sigma}u(t)+TL(y-CT^{-1}\underline{\psi}(t))+\\\qquad[(TD_{\sigma})^{+}\underline{\varpi}(t)-(TD_{\sigma})^{-}\bar{\varpi}(t)]+Tf_{\sigma}(t,\Delta\underline{x})+\underline{\eta}\end{cases} \tag{14}$$

where L is the observer gain matrix, $(TD)^{+}=\max\{0,TD\}$, $(TD)^{-}=(TD)^{+}-TD$, and it is easy to get $(TD)^{+}\geq 0$, $(TD)^{-}\geq 0$.

Theorem 1 The initial conditions are defined as $\underline{\psi}(0)=\min\{T\bar{x}(0),T\underline{x}(0)\}$, $\bar{\psi}(0)=\max\{T\bar{x}(0),T\underline{x}(0)\}$. If there exists a matrix L and such that $\Psi=T(A-LC)T^{-1}\geq 0$ with Schur stability, and the following inequality holds

$$\underline{\psi}(t)\leq\psi(t)\leq\bar{\psi}(t) \tag{15}$$

then system (14) is an interval observer for system (1) without actuator faults. T is an invertible constant matrix.

Proof: Define the upper bound error of the interval observer

$$\tilde{\bar{\psi}}(t)=\bar{\psi}(t)-\psi(t) \tag{16}$$

One can get

$$\begin{aligned}\dot{\tilde{\bar{\psi}}}(t)&=TA_{\sigma}T^{-1}\bar{\psi}(t)+T\Delta AT^{-1}\bar{\psi}(t)+TB_{\sigma}u(t)+\\&\quad TL(y-CT^{-1}\bar{\psi}(t))+[(TD_{\sigma})^{+}\bar{\varpi}(t)-(TD_{\sigma})^{-}\underline{\varpi}(t)]\\&\quad+Tf_{\sigma}(t,\Delta\bar{x})+\bar{\eta}-TA_{\sigma}T^{-1}\psi(t)-T\lambda(T^{-1}\psi,\Delta A)-\\&\quad TB_{\sigma}u(t)-TD_{\sigma}\omega(t)-Tf_{\sigma}(t,x)\\&=T(A-LC)T^{-1}\bar{\psi}(t)+TLCT^{-1}\psi(t)-TAT^{-1}\psi(t)\\&\quad+[(TD_{\sigma})^{+}\bar{\varpi}(t)-(TD_{\sigma})^{-}\underline{\varpi}(t)]-TD_{\sigma}\omega(t)+\\&\quad Tf_{\sigma}(t,\Delta\bar{x})-Tf_{\sigma}(t,x)+\bar{\eta}-T\lambda(T^{-1}\psi,\Delta A)\\&=T(A-LC)T^{-1}\tilde{\bar{\psi}}(t)+[(TD_{\sigma})^{+}\bar{\varpi}(t)-(TD_{\sigma})^{-}\underline{\varpi}(t)\\&\quad-TD_{\sigma}\omega(t)]+[Tf_{\sigma}(t,\Delta\bar{x})-Tf_{\sigma}(t,x)]+\\&\quad[\bar{\eta}-T\lambda(T^{-1}\psi,\Delta A)]\end{aligned} \tag{17}$$

According to Lemma 2, it follows that

$$\begin{aligned}&(TD)^{-}\underline{\omega}(t)\leq(TD)^{-}\omega(t)\leq(TD)^{-}\bar{\omega}(t),\\&(TD)^{+}\underline{\omega}(t)\leq(TD)^{+}\omega(t)\leq(TD)^{+}\bar{\omega}(t)\end{aligned} \tag{18}$$

According to Eq. (18), it is easy to obtain that

$$(TD_{\sigma})^{+}\bar{\varpi}(t)-(TD_{\sigma})^{-}\underline{\varpi}(t)-TD_{\sigma}\omega(t)\geq 0 \tag{19}$$

Under Assumption 3, there are

$$\begin{aligned}&Tf_{\sigma}(t,\bar{x})-Tf_{\sigma}(t,x)\geq 0,\\&Tf_{\sigma}(t,x)-Tf_{\sigma}(t,\underline{x})\geq 0\end{aligned} \tag{20}$$

It is easy to get

$$Tf_{\sigma}(t,\bar{x})-Tf_{\sigma}(t,x)-Tf_{\sigma}(t,\underline{x})\geq 0 \tag{21}$$

From Eq.(12), one can get

$$\bar{\eta}-T\lambda(T^{-1}\psi,\Delta A)\geq 0 \tag{22}$$

$$T\lambda(T^{-1}\psi,\Delta A)-\underline{\eta}\geq 0 \tag{23}$$

Similarly, $\underline{\eta}$ is easily obtained

$$\underline{\eta}-T\lambda(T^{-1}\psi,\Delta A)-\underline{\eta}\geq 0 \tag{24}$$

Since $\psi(t)=Tx(t)$,the initial state of system (11) satisfies

$$\underline{\psi}(0)\leq\psi(0)\leq\bar{\psi}(0) \tag{25}$$

i.e.

$$\tilde{\bar{\psi}}(0)=\bar{\psi}(0)-\psi(0)\geq 0 \tag{26}$$

It follows from Lemma 5 that for $\forall t\geq 0$, all the

$$\tilde{\bar{\psi}}(t)=\bar{\psi}(t)-\psi(t)\geq 0 \tag{27}$$

Similarly, defining the lower bound error $\tilde{\underline{\psi}}(t)=\psi(t)-\underset{\sim}{\psi}(t)$, it can be obtained that for $\forall t\geq 0$, there are

$$\tilde{\underline{\psi}}(t)=\psi(t)-\underset{\sim}{\psi}(t)\geq 0 \tag{28}$$

Thus, for any $t\geq 0$, there is $\underline{\psi}(t)\leq\psi(t)\leq\bar{\psi}(t)$, and then (14) is said to be the interval observer of the system (1) in the absence of actuator faults.

The Sylvester equation can be constructed from $\Xi=T(A-LC)T^{-1}$ as follows:

$$TA-\Xi T=QC, TL=Q \tag{29}$$

where Ξ is usually chosen as a diagonal matrix, and the unique solutions L and T can be obtained by solving equation (29) if and only if the matrix Ξ does not have common eigenvalues with matrix A.

The above interval observer is designed under the assumption that there is no actuator fault, i.e., $S_a(t)=0$. In this case, the upper and lower bounds of the output of the interval observer can be defined as

$$\begin{cases}\overline{y}(t)=\max\{C_iT^{-1}\overline{\psi}(t),C_iT^{-1}\underline{\psi}(t)\}\\ \underline{y}(t)=\min\{C_iT^{-1}\overline{\psi}(t),C_iT^{-1}\underline{\psi}(t)\}\end{cases} \tag{30}$$

That is, the actual output of the system without actuator faults should satisfy $\underline{y}(t)\le y(t)\le \overline{y}(t)$. The observer output error is defined as $\overline{e}_y(t)=\overline{y}(t)-y(t),\underline{e}_y(t)=y(t)-\underline{y}(t)$. Based on this, an interval observer-based fault detection mechanism is designed as follows:

$$\begin{cases} if\ \ \underline{e}_y(t)>0\ \ or\ \ \overline{e}_y(t)<0 & \Rightarrow fault=1\Rightarrow alarm\\ if\ \ \underline{e}_y(t)<0\ \ or\ \ \overline{e}_y(t)>0 & \Rightarrow fault=0\end{cases} \tag{31}$$

4. DESIGN OF ROBUST FAULT-TOLERANT CONTROL METHOD FOR INTERVAL DYNAMIC EVENT-TRIGGERED

In this section, the dynamic event interval trigger condition is given, and the interval dynamic condition based on the interval observer is designed on the basis of the conventional dynamic event triggered mechanism in order to obtain a longer triggering time interval compared with the conventional dynamic event triggering mechanism. The specific scheme adopted is as follows:

$$\begin{cases} t_0=0,\\ \tilde{t}_{k+1}=\inf\{t>t_k\mid \phi(t)+\partial(\varepsilon_1\|x(t)\|-\|e(t)\|)\le 0\\ and\mid x(t)-\hat{x}(t)\mid\ge\delta(t)\}\end{cases} \tag{32}$$

where $\partial>0,\hat{x}(t)=\dfrac{\overline{x}-\underline{x}}{2}$.

The dynamic variable $\phi(t),\delta(t)$ are defined as:

$$\dot{\phi}(t)=-\chi\phi(t)+\varepsilon_1\|x(t)\|-\|e(t)\| \tag{33}$$

$$\delta(t)=\alpha\|x(t)-\hat{x}(t)\|+\beta\|\overline{x}-\underline{x}\| \tag{34}$$

The Initial conditions are $\phi(0)\ge\phi_0,\chi>0,\alpha>0,\beta>0$.

The event-triggered error is defined as:

$$e(t)=x(\tilde{t}_k)-x(\tilde{t}_{k+1}) \tag{35}$$

where $\tilde{t}_k$ is the event-triggered transient. The k_{th} event-triggered instant $\tilde{t}_k$ is recorded and controller parameters are updated when the triggering condition in Eq. (32) is satisfied.

Remark 1 Compared with the traditional dynamic event triggered mechanism, (32) introduces new triggering conditions and dynamic variables $\delta(t)$, this enables the system to determine when to trigger more precisely when there is a large uncertainty, and reduces the probability of false or missed triggering. In the dynamic variable (34), α is the weighting factor of the observation error of the system state on the triggering condition, and an increase in α will make the triggered mechanism more sensitive to the observation error, thus improving the control accuracy. However, when α is too large, it may bring high communication and computation overhead. The range of estimated intervals of the system state, i.e., the width of the interval, is described by $\|\overline{x}-\underline{x}\|$, and is frequently utilized for the quantification of observer uncertainty or error range. β is the weighting factor of the influence of interval width on the trigger condition. By increasing β, the trigger mechanism can respond more frequently to changes in the observation error of the intervals, thus improving the adaptability to systems with fast dynamic changes and large uncertainties.

In this paper, it is considered that Eq. (32) will be applied to the robust fault-tolerant controller to be designed next. Assuming that n samples occur on the interval $[t_i,t_{i+1})$, then

$$u(t)=\begin{cases}u(\tilde{t}_k),t\in[t_i,\tilde{t}_{k+1})\\ u(\tilde{t}_{k+1}),t\in[\tilde{t}_{k+1},\tilde{t}_{k+2})\\ \cdots\\ u(\tilde{t}_{k+n}),t\in[\tilde{t}_{k+n},t_{i+1})\end{cases} \tag{36}$$

The following fault tolerant controllers are considered to be designed in this paper.

$$u(t)=K_ix(t)-B_i^{-1}E_i\hat{S}_a(t) \tag{37}$$

where $\hat{S}_a(t)$ is an adaptive estimate of the fault and is updated in the following form:

$$\dot{\hat{S}}_a(t)=E_iPx(t) \tag{38}$$

The actuator fault error function is defined as follows:

$$e_f(t)=S_a(t)-\hat{S}_a(t) \tag{39}$$

Theorem 2 For a given positive scalar μ,γ_0,ε, if there exist symmetric positive definite matrices *H*, *P* and control gain matrices *K*, such that the following inequality holds

$$\begin{bmatrix}\Theta_1 & PDi & \theta P & P & \Delta\overline{A}_i & C_i^T\\ * & -\gamma_0^{\ 2} & 0 & 0 & 0 & 0\\ * & * & -\frac{1}{\mu}I & 0 & 0 & 0\\ * & * & * & -\frac{1}{\varepsilon}H & 0 & 0\\ * & * & * & * & -\dfrac{\varepsilon}{\lambda_{\min}(H)} & 0\\ * & * & * & * & * & -I\end{bmatrix}<0 \tag{40}$$

then the closed-loop system (1) is globally asymptotically stable under any switched signal and has an H∞ performance index no greater than γ_0. That is

$$\int_0^t y^T(t)y(t)dt<\gamma_0^{\ 2}\int_0^t\omega^T(t)\omega(t)dt \tag{41}$$

where $\Theta_1 = (A_i + B_i K)^T P + P(A_i + B_i K) + \mu I$. $\lambda_{\min}(H)$ is defined as the minimum eigenvalue of the positive definite matrix *H*.

Proof: Choose a Lyapunov function

$$V_i(t) = x(t)^T Px(t) + e_f^{\ T}(t)e_f(t) \tag{42}$$

If the i_{th} subsystem is in the activated state, one can get

$$\begin{aligned}
&\dot{V}_i(t) + y^T(t)y(t) - \gamma_0^{\ 2}\omega^T(t)\omega(t) = \\
&\quad = \dot{x}^T(t)Px(t) + x^T(t)P\dot{x}(t) + y^T(t)y(t) \\
&\quad -\gamma_0^{\ 2}\omega^T(t)\omega(t) \\
&\quad = [(A_i + \Delta A_i)x(t) + B_i u(t) + D_i\omega(t) + \\
&\qquad f_i(t,x) + E_i S_a(t)]^T Px(t) + y^T(t)y(t) \\
&\qquad -\gamma_0^{\ 2}\omega^T(t)\omega(t) + x^T(t)P[(A_i + \Delta A_i)x(t) \\
&\qquad + B_i u(t) + D_i\omega(t) + f_i(t,x) + E_i S_a(t)] \ + \\
&\qquad x^T(t)PE_i^{\ T}e_f(t) + e_f^{\ T}(t)E_i Px(t)
\end{aligned} \tag{43}$$

Substituting into Eq. (37)-Eq. (39) yields

$$\begin{aligned}
&\dot{V}_i(t) + y^T(t)y(t) - \gamma_0^{\ 2}\omega^T(t)\omega(t) \\
&\ \le x^T(t)[(A_i + B_i K)^T P + P(A_i + B_i K) \\
&\ + \varepsilon\Delta A_i^T H^{-1}\Delta A_i + \frac{1}{\varepsilon}PHP]x(t) + y^T(t)y(t) \\
&\ -\gamma_0^{\ 2}\omega^T(t)\omega(t) + 2x^T(t)Pf_i(t,x) + 2x^T(t)PD_i\omega(t)
\end{aligned} \tag{44}$$

By Assumption 3 and Lemma 3, it can be shown that

$$2x^T(t)Pf_i(t,x) \le \frac{\theta^2}{\mu}x^T(t)P^T Px(t) + \mu x^T(t)x(t) \tag{45}$$

By Lemma 4, one can get

$$2x^T(t)PD_i\omega(t) \le \gamma_0^{\ 2}\omega^T(t)\omega(t) + \frac{1}{\gamma_0^{\ 2}}x^T(t)PD_i D_i^T Px(t) \tag{46}$$

Substituting Eq.(45) and Eq.(46) into Eq.(44), it is obtained that

$$\begin{aligned}
&\dot{V}_i(t) + y^T(t)y(t) - \gamma_0^{\ 2}\omega^T(t)\omega(t) \le \\
&\quad x^T(t)[(A_i + B_i K)^T P + P(A_i + B_i K) + \\
&\quad \varepsilon\Delta A_i^T H^{-1}\Delta A_i + \frac{1}{\varepsilon}PHP]x(t) + y^T(t)y(t) \\
&\quad -\gamma_0^{\ 2}\omega^T(t)\omega(t) + \frac{\theta^2}{\mu}x^T(t)PPx(t) + \\
&\quad \gamma_0^{\ 2}\omega^T(t)\omega(t) + \frac{1}{\gamma_0^{\ 2}}x^T(t)PD_i D_i^T Px(t) \\
&\quad + \mu x^T(t)x(t)
\end{aligned} \tag{47}$$

According to Eq.(47), one can get

$$\begin{aligned}
&\dot{V}_i(t) + y^T(t)y(t) - \gamma_0^{\ 2}\omega^T(t)\omega(t) \le \\
&\quad x^T(t)[(A_i + B_i K)^T P + P(A_i + B_i K) \\
&\quad + \varepsilon\Delta A_i^T H^{-1}\Delta A_i + \frac{1}{\varepsilon}PHP + \frac{1}{\gamma_0^{\ 2}}PD_i D_i^T P \\
&\quad + \frac{\theta^2}{\mu}PP + \mu I + C_i^T C_i + \frac{\varepsilon}{\lambda_{\min}(H)}\Delta A_i^T\Delta A_i]x(t) \\
&\quad = x^T(t)[(A_i + B_i K)^T P + P(A_i + B_i K) + \\
&\quad \varepsilon\Delta A_i^T H^{-1}\Delta A_i + \mu I + C_i^T C_i + \frac{\varepsilon}{\lambda_{\min}(H)}\Delta A_i^T\Delta A_i \\
&\quad + P(\frac{1}{\varepsilon}H + \frac{1}{\gamma_0^{\ 2}}D_i D_i^T + \frac{\theta^2}{\mu}I)P]x(t) = x^T(t)\Psi x(t)
\end{aligned} \tag{48}$$

i.e.

$$\dot{V}_i(t) + y^T(t)y(t) - \gamma_0^{\ 2}\omega^T(t)\omega(t) \le x^T(t)\Psi x(t) \le 0 \tag{49}$$

According to Eq.(49), combined with Schur complement,the following conclusions can be obtained.When Ψ satisfies the following condition

$$\Psi = \begin{bmatrix}
\Theta_1 & PDi & \theta P & P & \Delta\overline{A}_i & C_i^T \\
* & -\gamma_0^{\ 2} & 0 & 0 & 0 & 0 \\
* & * & -\frac{1}{\mu}I & 0 & 0 & 0 \\
* & * & * & -\frac{1}{\varepsilon}H & 0 & 0 \\
* & * & * & * & -\frac{\varepsilon}{\lambda_{\min}(H)} & 0 \\
* & * & * & * & * & -I
\end{bmatrix} < 0 \tag{50}$$

where $\Theta_1 = (A_i + B_i K)^T P + P(A_i + B_i K) + \mu I$, the closed-loop system (1) is asymptotically stable, and the H_∞ performance index is not greater than γ_0 .

5. EXPERIMENTAL SIMULATION

In order to verify the effectiveness of the proposed method, a simulation experiment study was carried out based on a system model of a variant vehicle with variable wing curvature in the literature (Zhu, Z. and Yu, J,2022) under the influence of multiple factors such as external perturbations, actuator failures and system uncertainties. The system model is described as follows:

$$\begin{cases}
\dot{x}(t) = (A_\sigma + \Delta A_\sigma)x(t) + B_\sigma u(t) + E_\sigma S_a(t) \\
\qquad + f_\sigma(x,t) + D_\sigma\omega(t) \\
y(t) = C_\sigma x(t)
\end{cases} \tag{51}$$

where $x(t) = [x_1(t), x_2(t), x_3(t), x_4(t)]^T = [\Delta V_0, \Delta\beta_0, \Delta\theta_0, \Delta q_0]^T$,

$V_0, \beta_0, \theta_0, q_0$ represent velocity (m/s), angle of attack (rad), pitch angle (rad) and pitch angle velocity (rad/s), respectively. The flight conditions of the morphing aircraft are assumed to be at an altitude of 1.5 km and an air temperature of 300 K. A morphing aircraft system with two subsystems is formed by considering the wing curvature c of 0% and 1%, which corresponds to the initial base wing state and the system states when the wing curvature is set to c=1% and c=0%, respectively. The attitude stability during the wing switched process is simulated and verified under a given initial velocity.

$$A(c) = \begin{bmatrix} -0.0003282c-0.00246 & 3.08c-3.903 & -9.8 & 0 \\ -0.0003766c-0.000067 & -0.000164c-0.9465 & 0 & 1 \\ 0 & 0 & 0 & 1 \\ 0.00821c+0.005878 & -4.6677 & 0 & 0 \end{bmatrix}$$

A(c) is the state matrix of the morphing aircraft model with the wing curvature change parameter c. The aircraft increases the wing curvature c by increasing the thickness of the upper surface of the wing, and the change of the state quantity caused by the wing curvature c changes the flight state. When the wing curvature c is 0% and 1%, the specific relevant matrix parameters are chosen as follows.

$$A_1 = A(0) = \begin{bmatrix} -0.00246 & -3.903 & -9.8 & 0 \\ -0.000067 & -0.9465 & 0 & 1 \\ 0 & 0 & 0 & 1 \\ 0.005878 & -4.6677 & 0 & 0 \end{bmatrix}$$

$$A_2 = A(1) = \begin{bmatrix} -0.002788 & -0.823 & -9.8 & 0 \\ -0.0004366 & -0.946664 & 0 & 1 \\ 0 & 0 & 0 & 1 \\ 0.014088 & -4.6677 & 0 & 0 \end{bmatrix}$$

$$B_1 = \begin{bmatrix} 0 & 0.0127 & 0 & 0 \\ -0.0596 & 0 & 0 & 0 \\ 0 & 0 & 0.1 & 0 \\ -21.45 & 0 & 0 & 0.1 \end{bmatrix}$$

$$B_2 = \begin{bmatrix} 0 & 0.0127 & 0 & 0 \\ -0.0596 & 0 & 0 & 0 \\ 0 & 0 & 0.1 & 0 \\ -21.45 & 0 & 0 & 0.1 \end{bmatrix}$$

$$C_1 = C_2 = \begin{bmatrix} 1 & 1 & 0 & 0 \\ 0 & 0 & 1 & 1 \end{bmatrix}, D_1 = D_2 = \begin{bmatrix} 0.5 \\ 0.5 \\ -0.5 \\ -0.5 \end{bmatrix}$$

$$E_1 = \begin{bmatrix} 1 & 0 & 0 & 0 \\ 0 & 0.1 & 0 & 0 \\ 0 & 0 & 0.9 & 0 \\ 0 & 0 & 0 & 0.1 \end{bmatrix}, E_2 = \begin{bmatrix} 1 & 0 & 0 & 0 \\ 0 & 0.5 & 0 & 0 \\ 0 & 0 & 1 & 0 \\ 0 & 0 & 0 & -0.1 \end{bmatrix}$$

Since A_1, A_2 are not nonnegative matrices, the interval observer (14) is designed after transforming the system accordingly by choosing Schur and nonnegative matrices Ξ and matrices Q respectively

$$\Xi = \begin{bmatrix} 0.27 & 0 & 0 & 0 \\ 0 & 0.11 & 0 & 0 \\ 0 & 0 & 0.61 & 0 \\ 0 & 0 & 0 & 0.14 \end{bmatrix}, Q = \begin{bmatrix} 1 & 0 \\ 0 & 1 \\ 1 & 1 \\ 0 & 1 \end{bmatrix}$$

The Sylvester's equation in Eq. (29) is solved to obtain

$$L_1 = \begin{bmatrix} -0.5827 & 2.6676 \\ 0.1825 & -2.6547 \\ 0.0217 & -11.7344 \\ -0.0076 & 10.0566 \end{bmatrix}, L_2 = \begin{bmatrix} -0.7436 & 3.1860 \\ 0.3298 & -3.0783 \\ 0.0591 & -11.6556 \\ -0.0246 & 9.9910 \end{bmatrix}$$

$$T_1 = \begin{bmatrix} 86.4427 & 199.4556 & 10.7975 & 46.4861 \\ 0.2419 & 0.5846 & -0.2602 & -0.1005 \\ -2.5021 & -2.5403 & -0.6551 & -0.6490 \\ 0.3319 & 0.7089 & 0.5994 & 0.9119 \end{bmatrix},$$

$$T_2 = \begin{bmatrix} 108.5924 & 353.9227 & 12.8313 & 79.5931 \\ 0.1275 & 0.4338 & -0.2734 & -0.1389 \\ -3.1387 & -4.5024 & -0.6951 & -1.0676 \\ 0.1620 & 0.4840 & 0.5749 & 0.8550 \end{bmatrix}$$

Based on **Theorem 2**, the control gain matrix of the robust fault-tolerant controller can be obtained as follows:

$$K_1 = \begin{bmatrix} 0.0081 & 41.9500 & 0.0161 & 0.0617 \\ -196.5349 & -78.7054 & -0.011 & 0.2222 \\ 0.0014 & 0.0096 & -24.9992 & -3.2806 \\ 1.7072 & -8997.416 & -3.2806 & -11.7675 \end{bmatrix},$$

$$K_2 = \begin{bmatrix} 0.0071 & 45.6130 & 0.0489 & -0.0787 \\ -213.7215 & -74.2714 & 0.0021 & 0.1986 \\ -0.000027 & 0.0292 & -27.1854 & 0.523 \\ 1.5026 & 9784.513 & 0.523 & -44.0718 \end{bmatrix}$$

In order to demonstrate the advantages of the proposed interval dynamic event-triggered robust fault-tolerant control scheme, the design results of the robust fault-tolerant control scheme based on static event-triggered mechanism, dynamic event-triggered mechanism, and interval dynamic triggered mechanism are shown in this section for comparison, respectively.

Case1:

The abrupt actuator fault in the system is defined as follows:

$$S_a(t)=\begin{cases}0, & t<1.\\ a_1\sin(2\pi\tilde{f}_1 t), & 1\le t<6.\\ a_2(1-e^{-2(t-3)}), & t\ge 6.\end{cases}$$

where $\tilde{f}_1=0.6, a_1=0.01, a_2=0.02$.

In addition, let

$f_1(t,x_1)=b_1x_1$, $f_2(t,x_2)=b_1x_2$, $\omega=b_1\cos(2\pi\tilde{f}_{11}t)$,

where $\tilde{f}_{11}=0.7, b_1=0.01$.

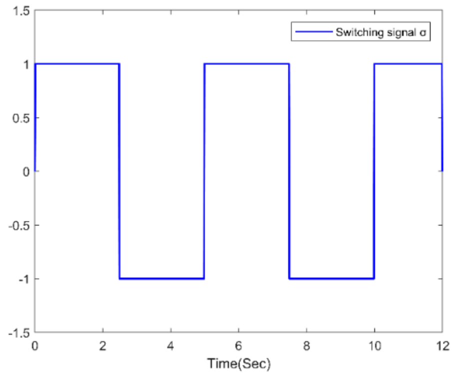

Fig. 1. Curve of switched signal $\sigma(t)$.

Under the initial conditions $x_1(0)=\begin{bmatrix}1 & 5 & -2 & -3\end{bmatrix}^T$, $x_2(0)=\begin{bmatrix}0.5 & 2.5 & -2.5 & -1\end{bmatrix}^T$, $\phi_0=0$, and the velocity V_0 is kept constant. The simulation results are shown in Fig.1-Fig.6.

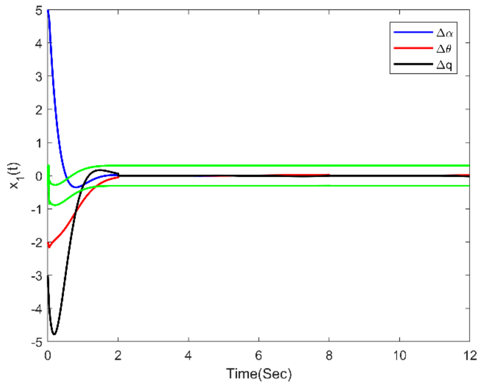

Fig. 2. State interval estimation for subsystem 1.

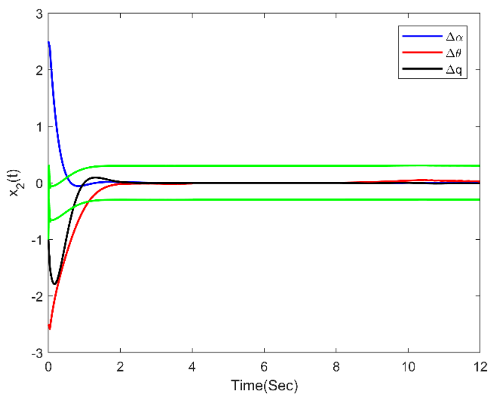

Fig. 3. State interval estimation for subsystem 2.

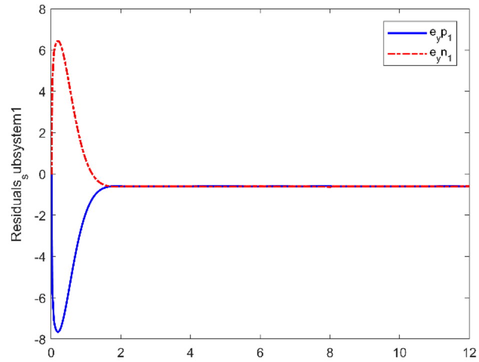

Fig. 4. Residual interval for subsystem 1.

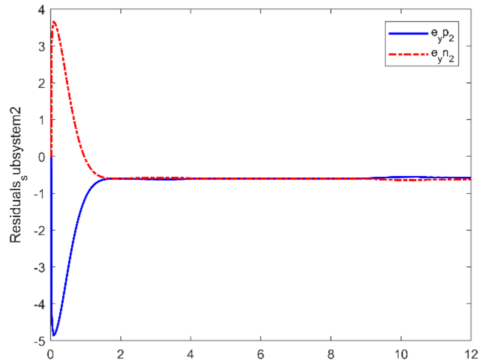

Fig. 5. Residual interval for subsystem 2.

The switched signal A is shown in Fig. 1, and the state response curves of the two subsystems of the variant vehicle under the action of the switched signal for wing curvature c=0% and c=1% are shown in Figs. 2 and 3, where the upper and lower bounds of the state estimation are represented by the green curves. The angle of attack, pitch angle, and pitch angle velocity are represented by $\Delta a, \Delta\theta, \Delta q$,respectively. The residuals of the system output with the upper and lower bounds of the interval observer are shown in Figs. 4-5. To evaluate the robustness of the proposed H∞ control framework, the H∞ performance index γ_0 is optimized to 0.17 via linear matrix inequalities, ensuring a balance between disturbance attenuation and control conservatism. According to the fault diagnosis mechanism (31), it can be seen that subsystem 1 is in a faulty state before 2.5s and subsystem 2 is in a faulty state before 4s. As can be seen from the figures, the effects of perturbations, uncertainties, and actuator failures can be effectively compensated by the designed control law, the good stability of the controlled morphing aircraft system is achieved when the wing curvature is switched.

When the event-triggered mechanism is not implemented, the number of data transmissions is recorded to reach 1200 times during a 12-second system operation. As demonstrated in Fig. 6(a), under the interval dynamic event-triggered mechanism, the two subsystems are observed to transmit data 126 and 164 times, representing reductions of approximately 89.5% and 86.3% in total transmission numbers, respectively. As illustrated in Fig. 6(b), under the dynamic event-triggered mechanism, data transmissions are recorded at 155 and 356 times for the two subsystems, corresponding to reductions of about 87% and 70.3% compared to the total transmission numbers.

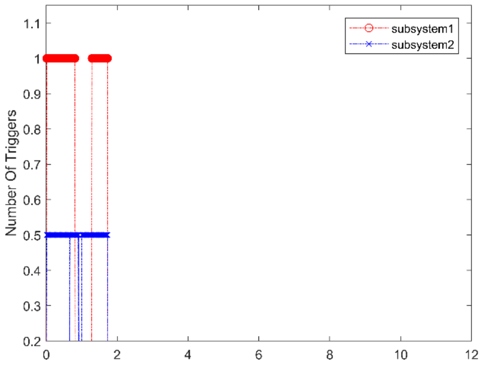

(a) Interval dynamic event-triggered mechanism

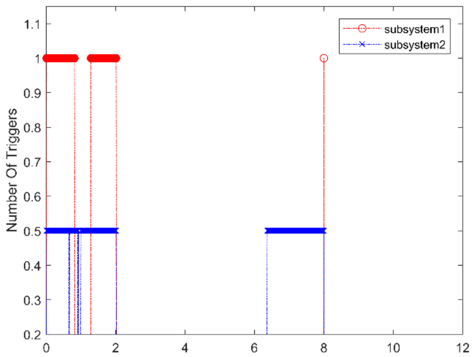

(b) Dynamic event-triggered mechanism

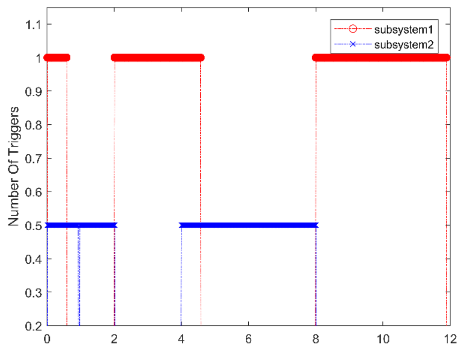

(c) Static event-triggered mechanism

Fig. 6. Numbers of trigger for interval dynamic event-triggered, dynamic event-triggered, and static event-triggered mechanisms.

As shown in Fig. 6(c), under the static event-triggered mechanism, the subsystems are measured to transmit data 727 and 612 times, indicating reductions of approximately 39.4% and 49% in total transmission numbers, respectively. While the desired system performance is maintained, the interval dynamic event-triggered mechanism is demonstrated to reduce data transmissions by 2.5%-16% compared to the dynamic event-triggered mechanism, and by 35%-37% compared to the static event-triggered mechanism, resulting in significant conservation of communication and computation resources.

Case 2:

The abrupt actuator faults in the system are defined as follows:

$$S_a(t)=\begin{cases}0, & t<1.5.\\ a_3\sin(2\pi\tilde{f}_2 t), & 1.5\le t<6.\\ a_4(1-e^{-2(t-3)}), & t\ge 6.\end{cases}$$

where $\tilde{f}_2=0.6, a_3=0.05, a_4=0.1$.

In addition, let

$$f_1(t,x_1)=b_2x_1\,,\ f_2(t,x_2)=b_2x_2\,,\ \omega=b_2\cos(2\pi\tilde{f}_{22}t)\,,$$

where $\tilde{f}_{22}=0.7, b_2=0.1$.

In order to check the robustness of the control system, by enhancing the faults, uncertainties, and perturbation amplitudes, the simulation results of the system operation under the initial condition of Case1 are shown in Fig.7-Fig.11.

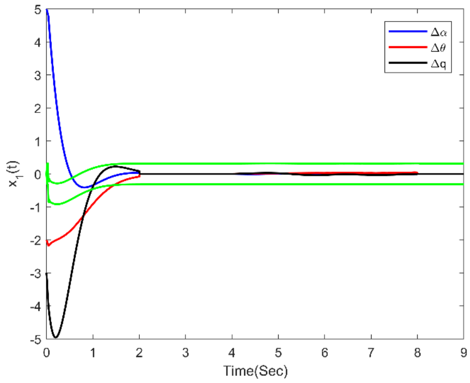

Fig. 7. State interval estimation for subsystem 1.

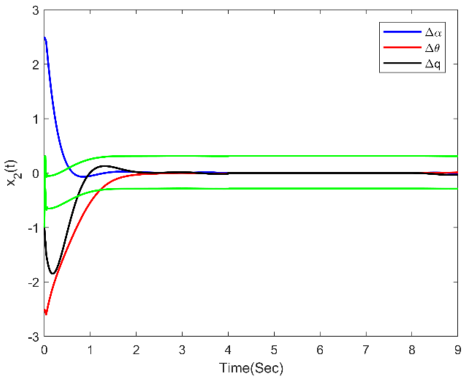

Fig. 8. State interval estimation for subsystem 2.

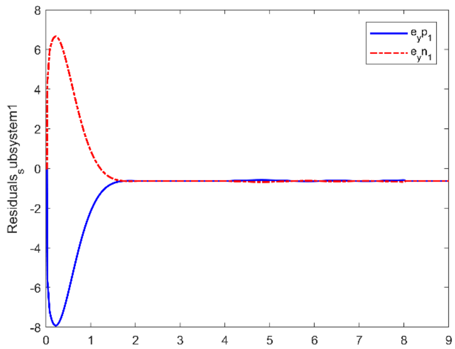

Fig. 9. Residual interval for subsystem 1.

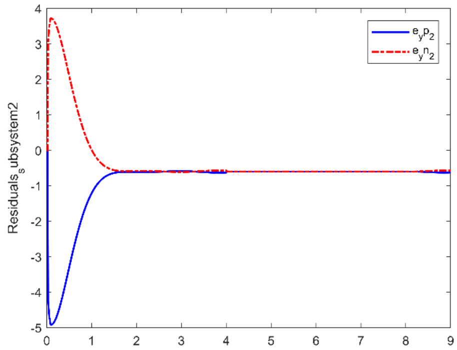

Fig. 10. Residual interval for subsystem 2.

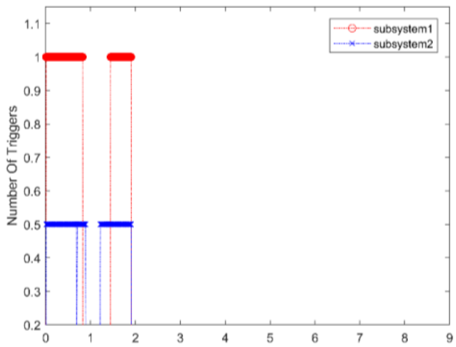

(a) Interval dynamic event-triggered mechanism

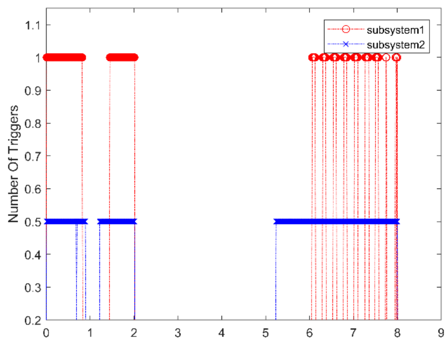

(b) Dynamic event-triggered mechanism

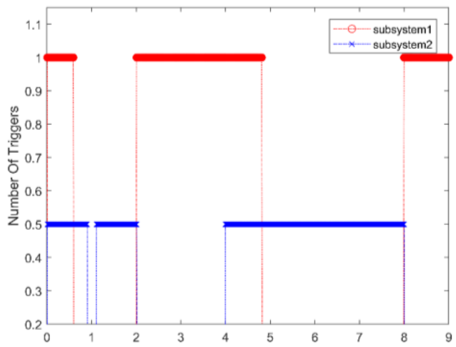

(c) Static event-triggered mechanism

Fig. 11. Numbers of trigger for interval dynamic event-triggered, dynamic event-triggered, and static event-triggered mechanisms.

By enhancing the disturbance uncertainty and the amplitude of the faults, the state curves of the angle of attack, pitch angle, and pitch angle velocity for the two subsystems of the morphing aircraft at wing camber values of c=0% and c=1% are illustrated in Figs. 7 and 8. The output residual intervals are shown in Figs. 9 and 10. It can be seen that the system is still able to converge quickly and has good performance.

In this scenario, the number of data transmissions is recorded to reach 900 times during a 9-second system operation when the event-triggered mechanism is not implemented. As demonstrated in Fig. 11(a), under the interval dynamic event-triggered mechanism, the two subsystems are observed to transmit data 128 and 157 times, representing reductions of approximately 85.7% and 82.5% in total transmission numbers, respectively. As illustrated in Fig. 11(b), under the dynamic event-triggered mechanism, data transmissions are recorded at 155 and 356 times for the two subsystems, corresponding to reductions of about 70.6% and 50.5% compared to the total transmission numbers. As shown in Fig. 11(c), under the static event-triggered mechanism, the subsystems are measured to transmit data 727 and 612 times, indicating reductions of approximately 19.2% and 32% in total transmission numbers, respectively. While the desired system performance is maintained, the interval dynamic event-triggered mechanism is demonstrated to reduce data transmissions by 11.9%-35.2% compared to the dynamic event-triggered mechanism, and by 47.3%-66.5% compared to the static event-triggered mechanism, resulting in effective conservation of communication and computation resources.

The simulation results demonstrate that the fault detection mechanism based on the interval observer proposed in this paper is capable of effectively discriminating the system fault state. When a fault is detected, the asymptotic stability of the variant vehicle wing curvature adjustment system is ensured by the robust fault-tolerant controller, which is designed based on the interval dynamic event triggering mechanism, while system robustness is maintained. A significant reduction in the consumption of communication and computational resources is achieved, thereby verifying the engineering applicability of the proposed approach in resource-constrained scenarios.

6. CONCLUSIONS

In this paper, the fault-tolerant control problem is investigated for a class of nonlinear switched systems in which model uncertainty and actuator faults coexist. Firstly, a mathematical model of the uncertain nonlinear switched system is established, and the effects of external disturbances and actuator faults are considered comprehensively. Secondly, an interval observer-based fault diagnosis method and an improved dynamic event-triggered robust fault-tolerant control strategy are proposed. The interval observer of uncertain switched system is constructed by coordinate transformation and Sylvester equation solution, and the fault diagnosis threshold criterion is designed based on the observer output. Further, the interval dynamic event-triggered mechanism with adaptive trigger threshold is proposed by integrating the interval estimation information and real-time residual analysis, which effectively prolongs the triggering interval and enhances the sensitivity of fault detection. On this basis, a robust fault-tolerant controller is designed based on the interval fault diagnosis results, and the stability of the closed-loop system is rigorously demonstrated. Finally, Sylvester's equation and linear matrix inequality are solved by MATLAB to obtain the gain matrices of the observer and the controller, respectively, and the designed fault diagnosis mechanism and fault-tolerant control method are applied to the nonlinear model of the wing curvature adjustment system of a variant vehicle, which verifies the validity of the proposed method in terms of resource saving and fault-tolerance performance.

ACKNOWLEDGEMENTS

This work is supported by National Natural Science Foundation of China under Grant 62103057.

REFERENCES

Ashraf, M.A., Ijaz, S., Javaid, U., Hussain, S., Anwaar, H., and Marey, M. (2021). A robust sensor and actuator fault tolerant control scheme for nonlinear system. *IEEE Access*, 10, 626–637.

Chen, T. and Francis, B.A. (2012). Optimal sampled-data control systems. *Springer Science & Business Media*.

Commault, C., Dion, J.M., Sename, O., and Motyeian, R. (2002). Observer-based fault detection and isolation for structured systems. *IEEE transactions on automatic control*, 47(12), 2074–2079.

Cui, D. and Xiang, Z. (2022). Nonsingular fixed-time fault tolerant fuzzy control for switched uncertain nonlinear systems. *IEEE Transactions on Fuzzy Systems*, 31(1), 174–183.

Ding, D., Wang, Z., and Han, Q.L. (2019). A set-membership approach to event-triggered filtering for general nonlinear systems over sensor networks. *IEEE Transactions on Automatic Control,* 65(4), 1792–1799.

Efimov, D. and Raïssi, T. (2016). Design of interval observers for uncertain dynamical systems. *Automation and Remote Control,* 77, 191–225.

Ge, X. and Han, Q.L. (2017). Distributed formation control of networked multi-agent systems using a dynamic event-triggered communication mechanism. *IEEE Transactions on Industrial Electronics,* 64(10), 8118–8127.

Girard, A. (2014). Dynamic triggering mechanisms for event-triggered control. *IEEE Transactions on Automatic Control,* 60(7), 1992–1997.

Guo, S. and Zhu, F. (2016). Actuator fault detection based on interval observers. *Control and Decision*, 31(6),1118–1122.

Guo, S. and Zhu, F. (2016b). Interval observers design for descriptor systems. *Control and Decision*, 31(2), 361-366.

Guo, S., Zhu, F., and Li, Z. (2019). Actuator fault detection for descriptor system: An interval observer approach. *Control Engineering of China*, 26(11), 2000-2005.

Han, J., Zhang, H., Wang, Y., and Liu, Y. (2015). Disturbance observer based fault estimation and dynamic output feedback fault tolerant control for fuzzy systems with local nonlinear models. *ISA transactions*, 59, 114–124.

Li, J., Pan, K., Zhang, D., and Su, Q. (2019). Robust fault detection and estimation observer design for switched systems. *Nonlinear Analysis: Hybrid Systems*, 34, 30– 42.

Liu, X., Han, J., Zhang, H., Sun, S., and Hu, X. (2019). Adaptive fault estimation and fault-tolerant control for nonlinear system with unknown nonlinear dynamic. *IEEE Access,* 7, 136720–136728.

Long, L. and Wang, F. (2021). Dynamic event-triggered adaptive NN control for switched uncertain nonlinear systems. *IEEE Transactions on Cybernetics*, 53(2), 988–999.

Long, L., Wang, F., and Chen, Z. (2022). Robust adaptive dynamic event-triggered control of switched nonlinear systems. *IEEE Transactions on Automatic Control*, 68(8), 4873–4887.

Ma, H., Li, H., Lu, R., and Huang, T. (2020). Adaptive event-triggered control for a class of nonlinear systems with periodic disturbances. *Science China Information Sciences*, 63, 1–15.

Ma, Y., Li, Z., and Zhao, J. (2020b). H_∞ control for switched systems based on dynamic event-triggered strategy and quantization under state-dependent switching. *IEEE Transactions on Circuits and Systems I: Regular Papers*, 67(9), 3175–3186.

Meseguer, J., Puig, V., Escobet, T., and Saludes, J. (2010). Observer gain effect in linear interval observer-based fault detection. *Journal of process control,* 20(8), 944–956.

Pourasghar, M., Puig, V., and Ocampo-Martinez, C. (2016). Characterization of the minimum detectable fault of interval observers by using set-invariance theory. *In 2016 3rd IEEE conference on control and fault-tolerant systems*, 79–86.

Qi, Y., Zhao, X., Fu, J., Zeng, P., and Yu, W. (2021). Event-triggered control for switched systems under multi-asynchronous switching. *IEEE Transactions on Systems, Man, and Cybernetics: Systems,* 52(7), 4685–4696.

Shuai, M., Yafeng, W., and Hua, Z. (2020). Parity-space-based FDI approach for advanced-aeroengine sensors. *In 2020 11th International Conference on Mechanical and Aerospace Engineering (ICMAE),* 140–144.

Szaszi, I., Kulcsar, B., Balas, G.J., and Bokor, J. (2002). Design of FDI filter for an aircraft control system. *Proceedings of the 2002 American Control Conference*, 5, 4232–4237.

Wang, X., Li, Y., Li, Y., Zhang, Q., and Chai, H. (2017). Closed-loop parity-space based fault detection: Application to simplified quadruped robot model. 2017 *Chinese Automation Congress (CAC*), 3015–3019.

Wu, Y., Zhang, J., and Fu, S. (2021). Non-fragile event-triggered control of positive switched systems with random nonlinearities and controller perturbations. *Bulletin of the Polish Academy of Sciences Technical Sciences*, e138566.

Xiao, X., Zhou, L., Ho, D.W., and Lu, G. (2018). Event-triggered control of continuous-time switched linear systems. *IEEE Transactions on Automatic Control*, 64(4), 1710–1717.

Zhang, Z.H. and Yang, G.H. (2018). Distributed fault detection and isolation for multiagent systems: An interval observer approach. *IEEE Transactions on Systems, Man, and Cybernetics: Systems*, 50(6), 2220–2230.

Zheng, Y., Fang, H., and Wang, Y. (2004). Kalman filter based FDI of networked control system. *Fifth World Congress* *on Intelligent Control and Automation (IEEE Cat. No. 04EX788)*, volume 2, 1330–1333.

Zhu, F., Shan, Y., Zhang, J., and Wang, F. (2020). Observer-based fault reconstructions and fault-tolerant control designs for uncertain switched systems with both actuator and sensor faults. *IET Control Theory & Applications,* 14(15), 2017–2029.

Zhu, F., Shan, Y., Zhang, J., and Wang, F. (2020). Observer-based fault reconstructions and fault-tolerant control designs for uncertain switched systems with both actuator and sensor faults. *IET Control Theory & Applications*, 14(15), 2017–2029.

Zhu, Z. and Yu, J. (2022). Anti-disturbance control of switching system and its application in variant aircraft. *Master's thesis,* Yangzhou University, Yangzhou,China.